LETTER

https://doi.org/10.1038/s41586-018-0106-2

# An unexpected and persistent increase in global emissions of ozone-depleting CFC-11

Stephen A. Montzka[1]*, Geoff S. Dutton[1,2], Pengfei Yu[2,3], Eric Ray[2,3], Robert W. Portmann[3], John S. Daniel[3], Lambert Kuijpers[4], Brad D. Hall[1], Debra Mondeel[1,2], Carolina Siso[1,2], J. David Nance[1,2], Matt Rigby[5], Alistair J. Manning[6], Lei Hu[1,2], Fred Moore[1,2], Ben R. Miller[1,2] & James W. Elkins[1]

**The Montreal Protocol was designed to protect the stratospheric ozone layer by enabling reductions in the abundance of ozone-depleting substances such as chlorofluorocarbons (CFCs) in the atmosphere[1–3]. The reduction in the atmospheric concentration of trichlorofluoromethane (CFC-11) has made the second-largest contribution to the decline in the total atmospheric concentration of ozone-depleting chlorine since the 1990s[1]. However, CFC-11 still contributes one-quarter of all chlorine reaching the stratosphere, and a timely recovery of the stratospheric ozone layer depends on a sustained decline in CFC-11 concentrations[1]. Here we show that the rate of decline of atmospheric CFC-11 concentrations observed at remote measurement sites was constant from 2002 to 2012, and then slowed by about 50 per cent after 2012. The observed slowdown in the decline of CFC-11 concentration was concurrent with a 50 per cent increase in the mean concentration difference observed between the Northern and Southern Hemispheres, and also with the emergence of strong correlations at the Mauna Loa Observatory between concentrations of CFC-11 and other chemicals associated with anthropogenic emissions. A simple model analysis of our findings suggests an increase in CFC-11 emissions of 13 ± 5 gigagrams per year (25 ± 13 per cent) since 2012, despite reported production being close to zero[4] since 2006. Our three-dimensional model simulations confirm the increase in CFC-11 emissions, but indicate that this increase may have been as much as 50 per cent smaller as a result of changes in stratospheric processes or dynamics. The increase in emission of CFC-11 appears unrelated to past production; this suggests unreported new production, which is inconsistent with the Montreal Protocol agreement to phase out global CFC production by 2010.**

Global production for dispersive uses of CFCs, the class of chemicals contributing most to atmospheric chlorine, was fully phased out[4] by 2010. In the absence of production, steady declines in CFC emissions are expected as the reservoir of chemicals remaining in existing equipment and products (CFC 'banks') gradually escapes to the atmosphere and diminishes. Declines in atmospheric concentrations follow when emission becomes smaller than atmospheric destruction. Expectations for the concentration of stratospheric ozone to return to 1980 levels by the middle of the 21st century rely on the continued decline in emissions and atmospheric concentrations (or mole fractions) of ozone-depleting gases, particularly CFCs.

For CFC-12 and CFC-113, two of the three most abundant CFCs, measured declines in atmospheric mole fractions over the past two decades have slowly approached lifetime-limited rates, which is consistent with diminishing production, emission and banks. Hemispheric mole-fraction differences, which arise because emissions are predominantly from the Northern Hemisphere, were also approaching zero[1].

For CFC-11, this conceptual framework explains the atmospheric changes observed from 1995 to 2002 reasonably well: production dropped below annual emissions, and the bank of CFC-11 (1,420 Gg in 2008, mostly in foams[5]) diminished, resulting in fewer emissions each year (Extended Data Table 1). After 2002, as reported production for all uses gradually decreased to zero, atmospheric rates of decline were projected to accelerate by a factor of 1.5 to 2 in response to the more rapid depletion of the CFC-11 foam bank[6,7] (Figs. 1, 2). However, accelerated atmospheric rates of decline were not observed: global CFC-11 mole fractions declined at a steady year-to-year rate[1,8] of $-2.1 \pm 0.3$ (1 s.d.) p.p.t. $yr^{-1}$ (or $-0.85 \pm 0.10\%$ $yr^{-1}$) in the decade after 2002 (p.p.t., parts per $10^{12}$; Fig. 1), which suggests a gap in our understanding of CFC-11 sources and sinks since the early 2000s.

The gap between expectations and observations widened substantially after 2012, when CFC-11 global mole fractions began decreasing even more slowly. In recent data (from mid-2015 to mid-2017), the mean rate of change for CFC-11 ($-1.0 \pm 0.2$ p.p.t. $yr^{-1}$, or $-0.4 \pm 0.1\%$ $yr^{-1}$) was about 50% slower than that observed during 2002–2012; it also was much slower than has been recently projected[7] (Fig. 1). This slowdown was observed by all three measurement systems at the National Oceanic and Atmospheric Administration (NOAA), and it was accompanied by a 50% increase in the mean hemispheric mole-fraction difference measured for CFC-11 (Fig. 1, Extended Data Fig. 1). The last time that hemispheric differences and global rates of change of these magnitudes were observed for CFC-11 was nearly two decades ago (Fig. 1b, c). Other long-lived gases do not show changes in global rates or hemispheric differences that are as large or as sustained as those observed for CFC-11 (Extended Data Fig. 2).

For long-lived chemicals emitted primarily in the Northern Hemisphere, concentration differences between hemispheres are highly correlated with global emission rates, although these differences are also influenced by rates of air exchange between the Northern and Southern Hemispheres and any hemispheric asymmetry in stratosphere–troposphere exchange (STE)[9]. Our analysis of other anthropogenically produced and emitted gases suggests no appreciable weakening in tropospheric Northern–Southern Hemisphere exchange in recent years (Extended Data Fig. 3), which indicates that the recent changes observed uniquely for CFC-11 are most likely to arise from a sustained increase in the net flux of CFC-11 to the troposphere of the Northern Hemisphere.

The slower global decline in CFC-11 mole fractions after 2012 represents a perturbation of around 20% in the balance of CFC-11 sources and sinks. When considered together, the observational evidence suggests an increase in CFC-11 emission in the Northern Hemisphere, a decrease in stratospheric loss rates or reduced STE primarily in the Northern Hemisphere, or some combination of these effects. When analysed with a three- or twelve-box model and constant tropospheric and STE dynamics, measured global atmospheric changes suggest a steady decrease in emissions in the 15 years before 2002 from a late-1980s peak of about 350 Gg $yr^{-1}$; relatively constant emissions from 2002 to 2012 at $54 \pm 3$ Gg $yr^{-1}$; and a mean emission rate during 2014–2016 of $67 \pm 3$ Gg $yr^{-1}$, which is $13 \pm 5$ Gg $yr^{-1}$

[1]Global Monitoring Division, Earth System Research Laboratory, National Oceanic and Atmospheric Administration, Boulder, CO, USA. [2]Cooperative Institute for Research in Environmental Sciences, University of Colorado, Boulder, CO, USA. [3]Chemical Sciences Division, Earth System Research Laboratory, National Oceanic and Atmospheric Administration, Boulder, CO, USA. [4]A/gent Consultancy BV, Venlo, The Netherlands. [5]School of Chemistry, University of Bristol, Bristol, UK. [6]United Kingdom Met Office, Exeter, UK. *e-mail: Stephen.A.Montzka@noaa.gov

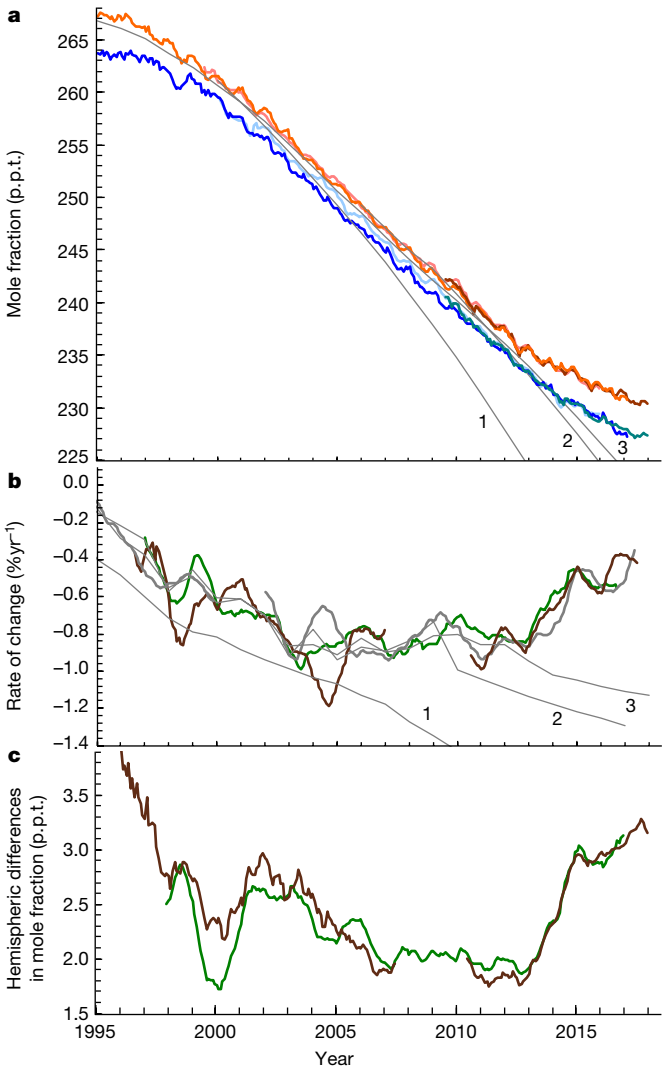


**Fig. 1 | Observations of atmospheric CFC-11 over time. a**, Hemispheric mean mole fractions estimated for the Northern (red lines) and Southern Hemispheres (blue lines); different shades of red or blue represent results from a total of three different instruments (see Methods). **b**, Inferred rate of change of the measured globally averaged mole fraction of CFC-11. **c**, Measured differences in hemispheric mean mole fraction of CFC-11 (North Hemisphere − South Hemisphere). In **b** and **c**, colours represent results from flask GC–MS (brown lines), flask GC–ECD (green lines) and, in **b** only, in situ GC–ECDs (thick grey lines). In **a** and **b**, the numbered thin grey lines represent projections from recent World Meteorological Organization (WMO) assessment scenarios (as global means) given the data available at the time the scenarios were created[6,7,26].

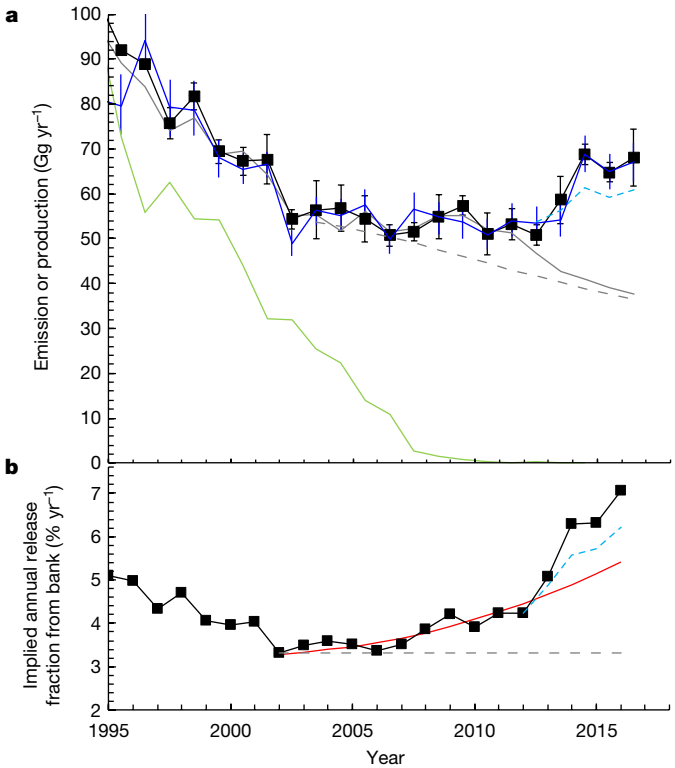


**Fig. 2 | Global CFC-11 emission, reported production and implied release rate from CFC-11 banks. a**, Production magnitudes reported to the United Nations Environment Programme[4] (UNEP, green line) are compared to emissions derived from atmospheric data with a three-box (black squares) or 12-box model (blue line) considering a 57.5-year lifetime (Extended Data Table 1). Also shown is an independent emission history, which is constrained by observations from NOAA and the Advanced Global Atmospheric Gases Experiment until the end of 2012, and thereafter is the WMO scenario projection[1,7] (grey solid line; rescaled for a 57.5-year lifetime). Uncertainties on three-box emissions represent 1 s.d. of the sum of squares of a bootstrap analysis plus the spread in estimates from several instruments (see Methods). **b**, The implied annual release fraction of CFC-11 from its banks, considering i) the UNEP production and three-box-derived emission histories in **a** (black squares; see Methods); ii) same as (i), but with the atmosphere-derived emission increase after 2012 reduced by 50% to represent potential dynamical contributions to that increase (blue dashed line in **a** and **b**); iii) a constant annual release fraction from the bank of 3.2% $yr^{-1}$ after 2002 (grey dashed lines); and iv) constant emissions at 54 Gg $yr^{-1}$ from 2002 to 2016 (red line). See also Extended Data Fig. 9.

(or 25 ± 13%) above the 2002–2012 mean (Fig. 2; see Methods). The post-2012 hemispheric differences and emission magnitudes are similar to those derived for the late 1990s, and are well represented by the three-box model (Extended Data Fig. 4). These results indicate consistency in two separate features of the measurements (trend and distribution) for all recent years, and support the conclusion that Northern Hemisphere emissions of CFC-11 have increased, although they do not rule out some contribution from changing stratospheric processes or STE dynamics.

Additional evidence for increasing CFC-11 emissions in the Northern Hemisphere after 2012 is provided by data from the Mauna Loa Observatory (MLO) in Hawaii. These data reveal the emergence of greater variability in CFC-11 mole fractions and of strong correlations between mole fractions of CFC-11 and other chemicals emitted from anthropogenic activity (Fig. 3, Extended Data Figs. 5–7). Trends in tropospheric ozone measured at MLO have revealed a considerable influence of emissions from Eurasia in autumn, when stratospheric influences are relatively small[10]. Autumn measurements from MLO reveal strong correlations between mole fractions of CFC-11 and mole fractions of anthropogenically produced gases that are emitted in substantial quantities, particularly from eastern Asia[1] (for example, HCFC-22 and $CH_2Cl_2$), with slopes roughly consistent with relative emission rates derived elsewhere for this region[11]. Back-trajectory analyses confirm that MLO sampling events that reveal increased mole fractions of these chemicals are associated with increased sensitivity to surface emissions from eastern Asia. Although similarly high correlations have been observed every autumn since 2009 at MLO between mole fractions of HCFC-22 and $CH_2Cl_2$ (and also between HCFC-22 and carbon monoxide), high correlations have been observed between CFC-11 and these pollution tracers only after 2012.

Although this evidence strongly suggests increased CFC-11 emissions from eastern Asia after 2012, changes in the CFC-11 lifetime or STE dynamics could influence the magnitude of emissions derived with the simple model approach. Given that the strength of stratospheric circulation can vary (for example, after the year 2000[12,13]), and considering recent documented changes in stratospheric transport

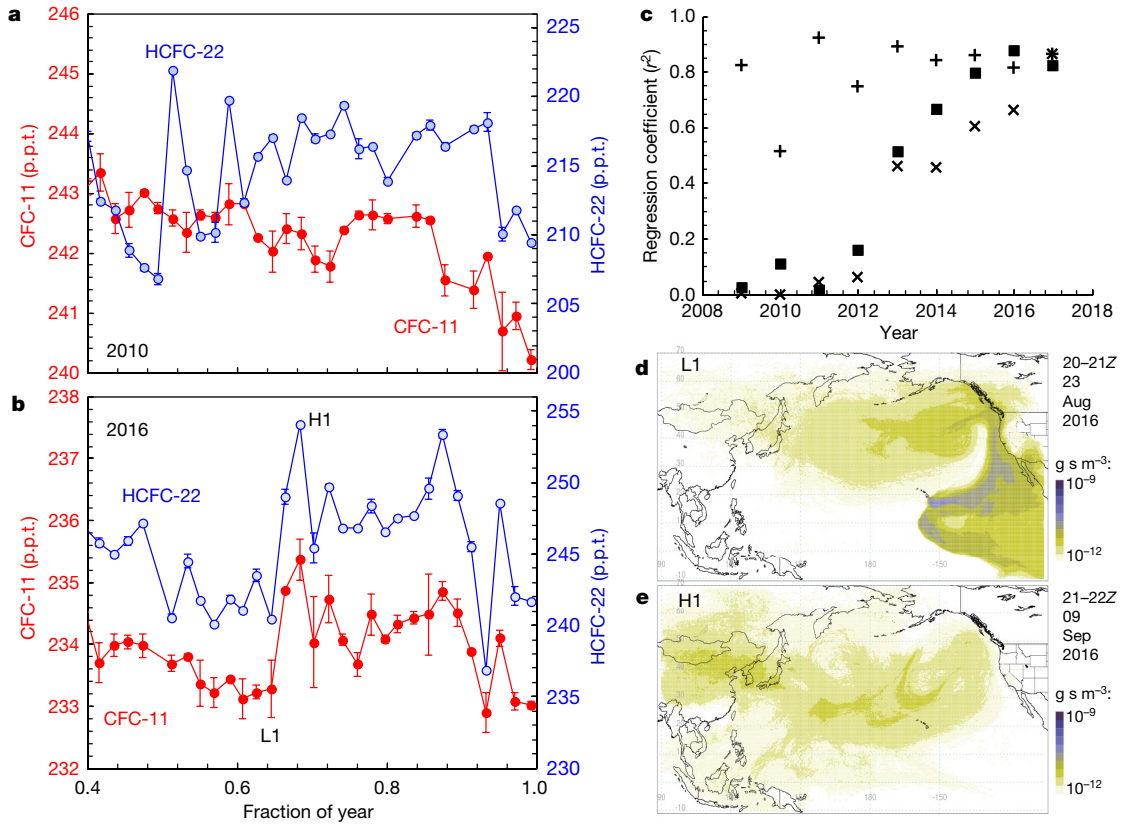


**Fig. 3 | Covariations in mole fractions of CFC-11 and HCFC-22 measured at MLO and air transport differences that influence this variability. a**, Mole fractions of CFC-11 and HCFC-22 measured by GC–MS in weekly flask pairs in 2010 at MLO; uncertainties represent 1 s.d. of flask pair means. **b**, Same as **a**, but for 2016. **c**, The annual regression coefficients ($r^2$) associated with results from MLO during autumn (fraction of year > 0.6 and < 0.9): CFC-11 versus HCFC-22 (squares), CFC-11 versus $CH_2Cl_2$ (crosses), and HCFC-22 versus $CH_2Cl_2$ (plus signs). **d**, **e**, A back-trajectory analysis[27] showing surface regions sensed by the 2016 sampling events at MLO labelled L1 and H1 in **b**, with darker colours indicating greater influence. Colour scale is logarithmic and represents the calculated time-averaged concentration within the surface layer (0–2000 m) during the 30 days before the sampling events given a point release at MLO of 1 g s$^{-1}$. See also Extended Data Figs. 5–7.

and STE[14–17] (including the presence of a substantial El Niño in late 2015 to early 2016, see https://www.esrl.noaa.gov/psd/enso/mei/), we simulated CFC-11 mole-fraction changes in two three-dimensional chemistry–climate models (CCMs), with three representations of reanalysed meteorology from 2000 to 2016 and, in some simulations, 2017 (refs 18–20; Methods).

When forward CCM simulations include the CFC-11 emission history derived from the three-box model, the rate of change simulated in the CCM for the global CFC-11 mole fraction is consistent with observations from 2000 to 2012. After 2012, however, a discrepancy becomes apparent, with simulated mole fractions declining more slowly (Fig. 4a, Extended Data Fig. 8). This discrepancy becomes much smaller when dynamics in 2012 are repeated in subsequent years, which suggests that changes in transport contributed to the slower decline observed for CFC-11 during 2014–2016; transport anomalies had a much smaller influence on the simulated rate of change in 2017. However, transport anomalies cannot entirely explain the slower decline observed after 2012, because simulated CFC-11 mole fractions decline too quickly in CCM runs in which emissions are kept constant after 2012.

Known uncertainties in CCMs and reanalysis meteorology[21] and model-dependent differences in our simulation results (Extended Data Fig. 8) preclude a robust estimate of dynamical influences on derived emissions. The comparison of observed rates of change to those simulated with constant and increasing emissions (Fig. 4a) suggests that the emission increase derived for 2014–2016 in the three-box model may be overestimated by as much as 50%.

We also considered CCM simulations of CFC-113 and CFC-12 (Extended Data Fig. 2). The CCM simulations showed no persistent bias throughout 2014–2016, which suggests that the mismatch observed for CFC-11 is unique.

Further evidence for increased CFC-11 emissions is provided upon considering changes in the hemispheric mole-fraction difference after 2012 (Fig. 4b, Extended Data Fig. 8). In all simulations in which emissions were kept constant after 2012, the simulated difference in mole fraction between the Northern and Southern Hemispheres did not increase, which suggests that the observed increase since then cannot be explained by changes in dynamics alone. Simulated hemispheric differences increase after 2012 analogously to observations only in response to increasing emissions, although the increase in hemispheric mole fraction difference was dependent on simulation details and was both smaller and larger in magnitude than those measured. Simulations that yield larger differences in mole fraction between the Northern and Southern Hemispheres than those observed would be more consistent with the post-2012 emissions increase being overestimated by the three-box analysis, but are derived only with emission distributions considered to be less likely in recent years (Methods). This apparent discrepancy may arise from simulated hemispheric mole-fraction differences being more sensitive to uncertain model details (for example, emission distribution) and simulated processes (for example, interhemispheric mixing timescales and STE) than are rates of change in globally averaged surface mole fractions (Fig. 4; Extended Data Fig. 8c, f, i).

It seems unlikely that the increased CFC-11 emissions are related to faster releases from banks or from inadvertent production. Increases in bank-related emissions are thought possible from the demolition of buildings that contain CFC products, although these emissions are expected to be small and only slowly increase over time[22]. Furthermore,

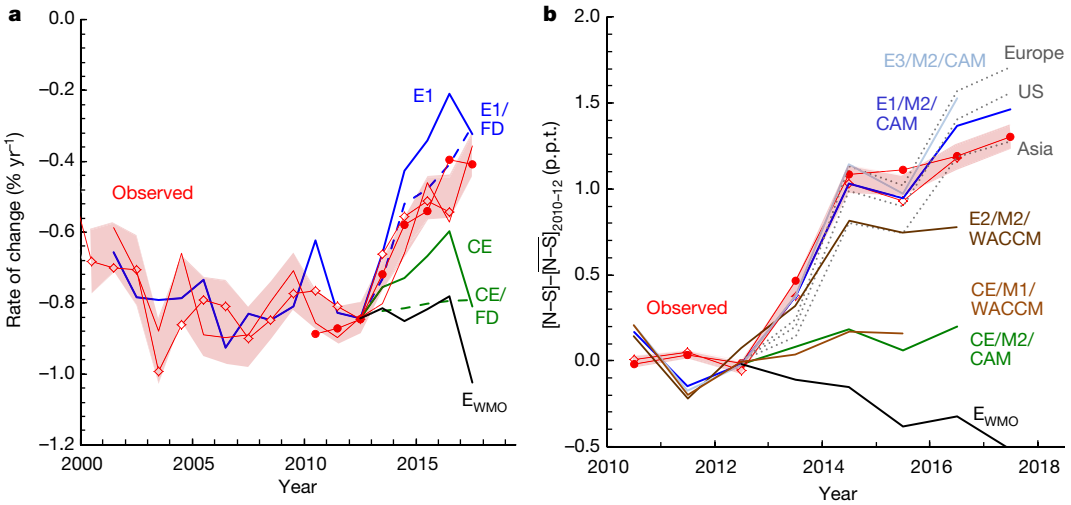


**Fig. 4 | Rates of change and hemispheric differences in the mole fraction of CFC-11. a**, Global rates of change of CFC-11 derived from observed (red symbols and lines; shaded region indicates 1 s.d. of 3-yr running mean in observations) or simulated (blue, green, black lines) mole fractions. Simulations were performed using the Community Atmosphere Model (CAM) CCM, the MERRA2 reanalysis meteorology (MERRA, Modern-Era Retrospective analysis for Research and Applications), and emission histories either from the three-box model (blue lines labelled E1) or E1 emissions kept constant at the 2012 rate after 2012 (green lines labelled CE). The simulation with the latest WMO emission projection[1] based on observations until the end of 2012 using the Whole Atmosphere Community Climate Model (WACCM) and MERRA1 reanalysis is shown as the black line. Simulations were also performed with 2012 dynamics applied to years after 2012 (dashed blue and green lines, labelled FD for fixed dynamics). **b**, The change since 2010 in observed and simulated hemispheric mole fraction difference (north minus south) relative to the 2010–2012 mean (note expanded *x*-axis scale). Colours in common with panel **a** refer to results obtained with those same methodologies, although only flask results are considered in **b**. CCM-simulation results are labelled as x/y/z, where x refers to how global emissions derived from the three-box model were distributed spatially (E1 = Emission1, and so on; see Methods), y refers to the reanalysis meteorology (M2, MERRA2; M1, MERRA1) and z refers to the model used. Additional dotted grey lines in **b** represent results from simulations with CAM and MERRA2 in which the entire post-2012 emission increase derived in the three-box model was distributed evenly throughout Europe, the United States (US) or Asia (see Methods and Extended Data Fig. 8). Observations are from flasks analysed by GC–ECD (red line, unfilled diamonds), GC–MS (red line, filled circles) and, in **a** only, in situ instrumentation (red line).

an increase in CFC emissions resulting from the decommissioning of buildings is anticipated to occur initially in developed countries in which most CFC-11 was used in the 1970s. However, atmospheric measurements suggest, for example, a decline in US emissions from 2008 to 2014, which is consistent with inventories[23] (a qualitative update suggests no substantial increases in emission after 2014). If reported production values are accurate, our results would require a doubling in the fractional release rate from CFC banks over the past 15 years and a substantial increase in emissions from banks since 2012, both of which seem improbable (Fig. 2b; Extended Data Fig. 9).

Inadvertent CFC-11 production is also possible from the fluorination of chlorinated methanes (for example, to produce HCFC-22), although we would expect this amount to be fairly small and that most, if not all, of the CFC-11 produced in this manner would be captured and recycled or destroyed.

These considerations suggest that the increased CFC-11 emissions arise from new production not reported to UNEP's Ozone Secretariat, which is inconsistent with the agreed phase-out of CFC production in the Montreal Protocol by 2010. Increased CFC-11 emissions augment the long-lived chlorine burden of the atmosphere and stratospheric ozone depletion rates. The recent emission increase has slowed the decline in total tropospheric chlorine by around 3 p.p.t. $yr^{-1}$ (approximately 22% considering 2008 to 2013 mean rate[1]) over the past three years. Other threats to stratospheric ozone that have been identified recently are substantially smaller[24] or relate to influences that could be reversed on short timescales[11,25]. This is the first time that emissions of one of the three most abundant, long-lived CFCs have increased for a sustained period since production controls took effect in the late 1980s. A delay in ozone recovery and enhanced climate forcing is anticipated, with an overall importance depending on the trajectory of CFC-11 emissions and concentrations in the future.

## Online content

Any Methods, including any statements of data availability and Nature Research reporting summaries, along with any additional references and Source Data files, are available in the online version of the paper at https://doi.org/10.1038/s41586-018-0106-2.

Received: 7 November 2017; Accepted: 19 March 2018;
Published online 16 May 2018.

1. Carpenter, L. J. et al. in *Scientific Assessment of Ozone Depletion: 2014*. Global Ozone Research and Monitoring Project—Report No. 55, Ch. 1, 1.1–1.101, (World Meteorological Organization, Geneva, 2014).
2. Montzka, S. A. et al. Decline in the tropospheric abundance of halogen from halocarbons: Implications for stratospheric ozone depletion. *Science* **272**, 1318–1322 (1996).
3. Prinn, R. G. et al. A history of chemically and radiatively important gases in air deduced from ALE/GAGE/AGAGE. *J. Geophys. Res.* **105**, 17751–17792 (2000).
4. Ozone Secretariat. *Handbook for the Montreal Protocol on Substances that Deplete the Ozone Layer*, 9th edn (United Nations Environment Programme, 2012).
5. Technology and Economic Assessment Panel. *Assessment of Alternatives to HCFCs and HFCs and Update of the TEAP 2005 Supplement Report Data*. Task Force Decision XX/8 Report (United Nations Environment Programme, Nairobi, 2009).
6. Daniel, J. et al. in *Scientific Assessment of Ozone Depletion: 2010*. Global Ozone Research and Monitoring Project—Report No. 52, Ch. 5, 5.1–5.56 (World Meteorological Organization, Geneva, 2011).
7. Harris, N. R. P. in et al. *Scientific Assessment of Ozone Depletion: 2014*. Global Ozone Research and Monitoring Project—Report No. 55, Chapter 5, 5.1–5.58 (World Meteorological Organization, Geneva, 2014).
8. Montzka, S. A. et al. in *Scientific Assessment of Ozone Depletion: 2010*. Global Ozone Research and Monitoring Project—Report No. 52, Chapter 1, 1.1–1.108 (World Meteorological Organization, Geneva, 2011).
9. Liang, Q. et al. Constraining the carbon tetrachloride ($CCl_4$) budget using its global trend and inter-hemispheric gradient. *Geophys. Res. Lett.* **41**, 5307–5315 (2014).
10. Lin, M., Horowitz, L. W., Oltmans, S. J., Fiore, A. M. & Fan, S. Tropospheric ozone trends at Mauna Loa Observatory tied to decadal climate variability. *Nat. Geosci.* **7**, 136–143 (2014).
11. Oram, D. E. et al. A growing threat to the ozone layer from short-lived anthropogenic chlorocarbons. *Atmos. Chem. Phys.* **17**, 11929–11941 (2017).

12. Rosenlof, K. R. & Reid, G. C. Trends in the temperature and water vapor content of the tropical lower stratosphere: Sea surface connection. *J. Geophys. Res.* **113**, D06107 (2008).
13. Randel, W. J., Wu, F., Vömel, H., Nedoluha, G. E. & Forster, P. Decreases in stratospheric water vapor after 2001: Links to changes in the tropical tropopause and the Brewer-Dobson circulation. *J. Geophys. Res.* **111**, D12312 (2006).
14. Ploeger, F. et al. Variability of stratospheric mean age of air and of the local effects of residual circulation and eddy mixing. *J. Geophys. Res.* **120**, 716–733 (2015).
15. Stiller, G. P. et al. Shift of subtropical transport barriers explains observed hemispheric asymmetry of decadal trends of age of air. *Atmos. Chem. Phys.* **17**, 11177–11192 (2017).
16. Newman, P. A., Coy, L., Pawson, S. & Lait, L. R. The anomalous change in the QBO in 2015–2016. *Geophys. Res. Lett.* **43**, 8791–8797 (2016).
17. Chirkov, M. et al. Global HCFC-22 measurements with MIPAS: retrieval, validation, global distribution and its evolution over 2005–2012. *Atmos. Chem. Phys.* **16**, 3345–3368 (2016).
18. Marsh, D. R. et al. Climate change from 1850 to 2005 simulated in CESM1(WACCM). *J. Clim.* **26**, 7372–7391 (2013).
19. Lamarque, J.-F. et al. CAM-chem: description and evaluation of interactive atmospheric chemistry in the Community Earth System Model. *Geosci. Model Dev.* **5**, 369–411 (2012).
20. Rienecker, M. M. et al. MERRA: NASA's modern-era retrospective analysis for research and applications. *J. Clim.* **24**, 3624–3648 (2011).
21. Boothe, A. C. & Homeyer, C. R. Global large-scale stratosphere-troposphere exchange in modern reanalyses. *Atmos. Chem. Phys.* **17**, 5537–5559 (2017).
22. Ashford, P. et al. in *Safeguarding the Ozone Layer and the Global Climate System: Issues Related to Hydrofluorocarbons and Perfluorocarbons* (eds Metz, B. et al.) Ch. 7 (Cambridge Univ. Press, Cambridge, 2005).
23. Hu, L. et al. Considerable contribution of the Montreal Protocol to declining greenhouse gas emissions from the United States. *Geophys. Res. Lett.* **44**, 8075–8083 (2017).
24. Laube, J. C. et al. Newly detected ozone-depleting substances in the atmosphere. *Nat. Geosci.* **7**, 266–269 (2014).
25. Hossaini, R. et al. The increasing threat to stratospheric ozone from dichloromethane. *Nat. Commun.* **8**, 15962 (2017).
26. Montzka, S. A. et al. in *Scientific Assessment of Ozone Depletion: 2002*. Global Ozone Research and Monitoring Project—Report No. 47, Ch. 1, 1.1–1.83 (World Meteorological Organization, Geneva, 2003).
27. Jones, A. R., Thomson, D. J., Hort, M. & Devenish, B. in *Air Pollution Modeling and its Application* XVII (eds Borrego C. & Norman A.-L.) Ch. 62, 580–589 (Springer, New York, 2007).

**Acknowledgements** We thank NOAA station personnel for sample flask collection and on-site instrument operation, maintenance and troubleshooting; and personnel from cooperative institutions involved with flask sampling in Australia (CSIRO), Canada (AES), Ireland (University of Bristol), Israel (Weizmann Institute) and the United States (University of Colorado, Harvard University, University of Wisconsin, and the Scripps Institute for Oceanography). We thank the US National Science Foundation for logistics support at Summit (Greenland) and the South Pole; J. Butler, D. Fahey, S. Reimann, P. Newman and scientists from the Advanced Global Atmospheric Gases Experiment for discussions; S. Davis for MERRA2 reanalysis winds; and P. Novelli for CO data from MLO. The CESM project is supported by the NSF and the Office of Science (BER) of the US Department of Energy. We acknowledge the NOAA Research and Development High Performance Computing Program for computing and storage resources. This work was funded in part by the NOAA Climate Program Office's AC4 program. The scientific results and conclusions, as well as any views or opinions expressed herein, are those of the authors and do not necessarily reflect the views of NOAA or the Department of Commerce.

**Reviewer information** *Nature* thanks J. Laube and the other anonymous reviewer(s) for their contribution to the peer review of this work.

**Author contributions** S.A.M. led the investigation, provided GC–MS measurements, and performed interpretive analysis and box modelling; G.S.D., D.J.N. and D.M. provided GC–ECD measurements; C.S. and B.R.M. provided GC–MS measurements; D.J.N. and M.R. performed 12-box modelling; P.Y. and R.W.P. performed CCM simulations; J.S.D., E.R. and F.M. performed box modelling and provided conceptual understanding; B.D.H. ensured accuracy and consistency in standard scales; L.K. provided insight into UNEP reporting; L.H. provided data analysis; A.J.M. performed trajectory calculations; and S.A.M. wrote the paper with input from J.S.D., M.R., P.Y., L.K., B.D.H., G.S.D., J.W.E. and L.H.

**Competing interests** The authors declare no competing interests.

**Additional information**
**Extended data** is available for this paper at https://doi.org/10.1038/s41586-018-0106-2.
**Reprints and permissions information** is available at http://www.nature.com/reprints.
**Correspondence and requests for materials** should be addressed to S.A.M.
**Publisher's note:** Springer Nature remains neutral with regard to jurisdictional claims in published maps and institutional affiliations.

## METHODS

**Observations.** We have measured CFCs and other trace gases in ambient air at several sites across the globe for over two decades by three different methods[1,2] (Extended Data Table 1). At two remote sites in the Southern Hemisphere and four remote sites in the Northern Hemisphere, air is collected and analysed several times per day by automated onsite instrumentation with gas chromatography coupled with electron capture detection (GC–ECD). At those and other remote sites (12 in total), paired glass or stainless-steel flasks are collected approximately weekly when winds are from a clean air sector. These flasks are analysed in our laboratories in Boulder on two separate gas chromatography instruments using different columns and detectors: separation on a 10% SP-2100 packed column followed by ECD, and separation on a 60 m, 0.25 mm internal diameter capillary column with a 1 μm DB-5 film thickness followed by mass spectrometry detection (GC–MS), primarily on ion $C^{35}Cl^{37}ClF^{+}$ ($m/z = 103$). Flask air has also been analysed on additional GC–MS instruments using a 0.32 mm ID GasPro column. Results from these instruments show similar distributions, rates of change and trace-gas correlations, so are not discussed further.

Consistency over time in the GC–MS standard scale is maintained independently from GC–ECD instruments. For GC–MS data, the scale is maintained by the sequential analysis of a suite of high-pressure real-air samples in treated aluminium cylinders. Consistency in that scale is assessed by repeat analysis of real humidified air in a separate suite of eight high-pressure, electropolished stainless steel cylinders, and is estimated to be better than 0.1 p.p.t. over 2010–2017. A measure of the consistency in results from GC–ECD instrumentation (field instruments and the flask analysis instrument) is provided by repeat analyses of gravimetrically prepared standards and an independent suite of high-pressure real-air samples on a common laboratory-based ECD instrument in Boulder; it is estimated to be 0.2 p.p.t. (1 s.d.) over the 2010–2017 period.

Results from all three measurement systems are tied to a suite of standards prepared in-house with gravimetric techniques[28] spanning 100–260 p.p.t. CFC-11. These standards enable the accurate characterization of instrument response over the range of measured ambient CFC-11 mole fractions. Comparisons with other global observations[1] indicated NOAA ECD results for CFC-11 declining around 0.2 p.p.t. $yr^{-1}$ faster than those from one international sampling program from 2008 to 2012 (the Advanced Global Atmospheric Gases Experiment[3]), although this divergence has become negligible with the NOAA ECD CFC-11 scale revision in 2016.

GC–MS measurements from flasks improved considerably after a detector upgrade in 2009 (median flask pair agreement was 0.4 p.p.t. before 2009 and has been 0.25 p.p.t. (or 0.1%) afterwards). GC–MS results from mid-2008 to mid-2009 suffer from detector problems, so we focus here on post-2009 data from this instrument.

**Data treatment.** Monthly mean mole fractions are derived from flask pairs sampled during the month; the small fraction (typically < 5%) of results deemed unrepresentative of the background atmosphere based on variability in sequential measurements and results from nearby sites are not considered additionally. Hemispheric means are derived by weighting results by cosine of sampling latitude, except for the South Pole, for which a weight of 0.4 is used to give South Pole results an equivalent weight to those from Palmer Station. In our experience results from these sites are similarly representative of CFC mole fractions in the high-latitude Southern Hemisphere.

The global rate of change quoted for CFC-11 mole fractions during 2002–2012 is the mean and 1 s.d. of the ten year-to-year differences measured for the global mean surface mole fraction (relative rates determined as $\ln(\text{mean}_{y2}/\text{mean}_{y1})$). In all figures, rates and hemispheric mole fraction differences are displayed as running 12-month means; rates are plotted at the end of the 12-month intervals. We consider hemispheric differences estimated only from flask measurements, because small intersite differences are more reliably determined when samples from different sites are analysed with a single instrument and because the estimates are more accurate when derived from the larger number of flask collection sites.

**Three-box model for deriving emissions.** Calculations were performed with a three-box model with boxes representing the Northern- and Southern Hemisphere troposphere, separated at the equator, and the stratosphere. The model includes a timescale for exchange between tropospheric boxes of 1.1 yr, a timescale for mass exchange between the stratosphere and troposphere of 2 yr (with 55% occurring in the Northern Hemisphere and 45% in the Southern Hemisphere), although our conclusions do not depend strongly on these particular values. Emissions were distributed so that 95% were in the Northern Hemisphere troposphere[29,30]. The loss rate constant in the stratospheric box was adjusted to provide a steady-state lifetime matching the mean CFC-11 lifetime diagnosed in the CCMs (56, 57.5 or 62 yr depending on model). Although these lifetimes are slightly longer than the best estimate (52(43–67) yr, ref. 1), they are well within this range. Emissions derived with this model are indistinguishable from those derived with other models when similar observations and lifetimes are considered[1,31] (Fig. 2).

Uncertainties in measurement-based estimates of global annual mean mole fractions affect our ability to assess changes in emissions over time. In GC–MS flask results, site-specific standard deviations of monthly means ranged between 0.08 to 0.14% (1 s.d.) at the 12 remote sites used in this study when averaged over 2010–2017; the variability in sequential monthly means at these sites is another measure of uncertainty and is even smaller (0.02 to 0.04%, 1 s.d.). Uncertainties of global annual means were estimated with a bootstrap technique using replacement. This involved the estimation of global annual mean mole fractions from a random selection of sites in the network, and uncertainties of monthly site means were also included. The only requirement of each randomly selected network was that it include > 1 Southern Hemisphere site. Uncertainties (1 s.d.) of these global means ranged from 0.1 to 0.2 p.p.t. (0.05 to 0.1%), which corresponds to an annual emission uncertainty (1 s.d.) ranging from 1.5 to 3 Gg $yr^{-1}$.

The difference between average emissions derived during 2002–2012 and 2014–2016 was estimated to be $13 \pm 5$ Gg. The uncertainty on this value includes $\pm 1.5$ Gg for a CFC-11 lifetime range of 43–67 yr (ref. 1). Additional error included in the $\pm 5$ Gg uncertainty was estimated with three different approaches that yielded consistent values: from the sum of squares of emission variability in mean emissions derived for these two periods with the three-box model from the three instrumental methods; from those derived from a bootstrap analysis of global annual mean uncertainties (discussed above); and from those derived from the 12-box model (see below).

The relative uncertainty in the emission increase (that is, when stated relative to the mean 2002–2012 emission) includes a lifetime dependence on the pre-2013 emissions assuming a lifetime of 57.5 yr and an error associated with loss derived for the lifetime range quoted above. When derived with a 52-yr lifetime, the mean emission during 2014–2016 is estimated to be $21 \pm 11\%$ higher than mean emissions during 2002–2012.

Uncertainty related to the accuracy of the surface network to represent full tropospheric mean mole fractions and their change over time was assessed with CCMs. The bias is a function of emission magnitude and, when averaged over 2014–2016, was approximately + 1 Gg $yr^{-1}$, or well within the uncertainties listed in Extended Data Table 1 and those on the derived emission increase. Consideration of CCM results also suggests that mean hemispheric mole fraction differences estimated from our sampling network overestimate the tropospheric column hemispheric difference in all years by 0.5 to 0.75 p.p.t. This bias is substantially reduced (0.2 p.p.t.) when hemispheric mole fraction differences (north minus south) are considered relative to the 2010–2012 mean. As a result, all comparisons performed between measurement-based and CCM-simulated hemispheric mole-fraction differences (for example, Fig. 4 and Extended Data Fig. 8) were performed by extracting mole fractions from CCM-simulated mole fraction fields at site-specific locations and treating those results as we did observations to derive hemispheric and global means. Furthermore, considering changes in the Northern and Southern Hemisphere differences relative to the 2010–2012 mean minimizes errors associated with the spatial distribution of pre-2012 CFC-11 emissions on our analysis (for example, see Extended Data Fig. 8). Finally, changes in site-derived hemispheric differences were found to be very consistent with hemispheric differences when derived from simulated mole fractions in all near-surface model grid cells.

Emission histories were similarly derived for CFC-12 and CFC-113 using our observations, the three-box model and lifetimes matching those diagnosed in the CCMs. Those emission histories were also used as input in forward runs of the CCM simulations. These gases were considered during assessment of the CCM simulations even though STE influences on tropospheric mole fractions are dependent on chemical lifetime.

**Bank release rate calculation.** The annual release fraction of CFC-11 from its banks was derived from the emission and production histories shown in Fig. 1 and a CFC-11 bank totalling 1,420 Gg in 2008 (ref. 5). The absolute value of this rate is dependent on the CFC-11 lifetime. An analysis of emission histories derived for lifetimes within the most likely range (43–67 yr) suggests a lifetime-independent conclusion: if the CFC-11 production history is accurate, the annual bank release rate would have had to approximately double during the past decade in the absence of unreported production (Extended Data Fig. 9). Considering the reporting to UNEP of quantities of CFC-11 that have been destroyed does not change this conclusion (Extended Data Fig. 9). Given the unlikely potential for this substantial increase, we conclude that the emission increase is more likely to result from unreported production.

**12-box model for deriving emissions.** Estimates of CFC-11 emissions were also made using a two-dimensional, 12-box model of atmospheric transport and chemistry and observations from ECD measurements or from GC–MS data[31]. In each vertical level, the model consists of four equal-mass boxes separated at 30 degrees north and south and at the equator. Vertical divisions are at 500 hPa and 200 hPa. Stratospheric loss rates were tuned such that the annual-mean global lifetime was 56 yr, consistent with 3D model predictions. Emissions were estimated for each season in each model semi-hemisphere between 1994 and 2016, using a

least-squares fit to the data (that is, with no prior constraint on the emissions). Model transport parameters were tuned to produce similar semi-hemispheric background mole fractions to long-term means in a 3D model and were assumed to be interannually repeating[31]. Monthly, semi-hemispheric means were calculated from the data for comparison with the model. The uncertainty on each of these averages was assumed to be the quadratic sum of the measurement repeatability and the variance in the observed monthly averages across sites within each semi-hemisphere. The latter term represents an estimate of the model 'mismatch' error, which was here assumed to be due to the lack of spatial resolution in the model. No systematic uncertainties were included in the emissions uncertainty estimate (for example, uncertainties due to lifetime or calibration scales), because the primary focus of this work is to understand changes in inferred emissions, rather than their absolute magnitudes; uncertainties related to variations in transport and transport-derived changes in loss are considered in the CCM simulations. The emission uncertainties calculated in this manner were similar to those calculated from the bootstrap analysis of the observations in the three-box model analysis.

**Chemistry–climate model simulations.** CCM simulations were performed to assess the role of changing atmospheric processes (chemistry and dynamics) on CFC-11 mole fractions. Biases noted between observed mole fractions and those from CCM simulations potentially indicate changes in atmospheric dynamics; such influences also became apparent from simulations performed with repeating reanalysis meteorology.

CFC-11 mole fraction histories were calculated in forward simulations in WACCM[18] and the CAM 5.3 (ref. 19) of the Community Earth System Model (CESM1), version 1. Models were run at 1.9° latitude × 2.5° longitude horizontal resolution with 88 vertical levels from Earth's surface to $6 \times 10^{-6}$ hPa. Horizontal winds and temperatures are nudged to specified dynamics derived from three different reanalysis products including MERRA[20], MERRA2 and the Goddard Earth Observing System Data Assimilation System Version 5 (GEOS5). A separate run in which the model winds only were nudged (not temperature) was also performed with MERRA2 in CAM5 (wind-only nudge results in Extended Data Fig. 8).

Global mole fractions and distributions of CFC-11 and other CFCs were initialized in the year 2000. Three different emission histories were considered thereafter: 1) emissions estimated from the three-box analysis of observations for all years given a steady-state lifetime matching that diagnosed from the particular CCM and meteorology; 2) same as in case 1, but with emissions kept constant during 2013–2016 at 2012 rates; and, for CFC-11 only, 3) emissions projected from the most recent WMO Ozone Assessment[1] (rescaled to the lifetime considered here). Emission magnitudes used for 2017 simulations were assumed to be unchanged from 2016 values, given that the observational data required to derive 2017 emissions are not yet available (data through mid-2018 are required with the existing methodology).

Multiple spatial distributions of CFC-11 emissions were also used in CCM simulations to test the sensitivity of simulated hemispheric difference on those distributions. The distributions include a span of 90 to 96.1% in the fraction of total emission from the Northern Hemisphere (or 85 to 95% in the fraction of emission north of 10° N), which encompasses previous estimates based on production data[29,30]. Total global emissions were distributed in each year as follows: Emission1, evenly distributed across land surfaces in the zonal bands as follows: 0% from 90° N to 60° N, 5% from 60° N–50° N, 80% from 50° N–25° N, 12% from 25° N–10° S, 3% from 10° S–40° S, 0% from 40° S–90° S (equivalent to 90% of emission north of 10° N); Emission2, 0% from 90° N to 60° N, 5% from 60° N–50° N, 80% from 40° N–10° N, 10% from 10° N–10° S, 5% from 10° S–40° S, 0% from 40° S–90° S (equivalent to 85% of emission north of 10° N); and Emission3, the GEIA emission distribution[30] (equivalent to 95% of emission north of 10° N). The sensitivity of emission location on our simulated results was also tested in three 'tagged-tracer' experiments in which the CFC-11 emission magnitude above the 2010–2012 average was distributed evenly in years after 2012 throughout regions representing Asia (20° N–40° N, 90° E–120° E), the United States (20° N–50° N, 60° W–120° W) or Europe (30° N–60° N, 0–60° E); emissions in other regions in these simulations were kept constant after 2012 (Fig. 4).

Although accurate spatial distributions of CFC-11 emissions are not well defined, they are estimated on the basis of country-scale reporting of CFC production and consumption to UNEP[4]. Given the phase-out of CFC production first in developed countries, the CFC-11 emission distribution has probably shifted to more southerly latitudes over time[29,30] and, therefore, become more like distribution Emission2 (or the Asian region in tagged tracer experiments) rather than that prescribed in Emission1 or Emission3.

Whereas the post-2012 emission increase in the Northern Hemisphere averaged 13 Gg during 2014–2016 in these tagged-tracer simulations, the Northern Hemisphere emission increase was smaller (by up to 2 Gg) in the simulations using emission distributions 1, 2, and 3 because these runs did not consider a changing emission distribution. Emissions of CFC-12 and CFC-113 were distributed as in Emission1. Rates of change simulated for CFC-11 mole fraction with the three-box-model-derived emissions were insensitive to lifetime, but had some dependence on the model and choice of meteorology and nudging methodology (Extended Data Fig. 8a, d, h).

**Data availability.** Data used in this study are available at ftp://ftp.cmdl.noaa.gov/hats/cfcs/cfc11/ or from the corresponding author upon reasonable request.


28. Hall, B. D., Dutton, G. S. & Elkins, J. W. The NOAA nitrous oxide standard scale for atmospheric observations. *J. Geophys. Res.* **112**, D09305 (2007).
29. McCulloch, A., Ashford, P. & Midgley, P. M. Historic emissions of fluorotrichloromethane (CFC-11) based on a market survey. *Atmos. Environ.* **35**, 4387–4397 (2001).
30. Liang, Q., Stolarski, R. S., Douglass, A. R., Newman, P. A. & Nielsen, J. E. Evaluation of emissions and transport of CFCs using surface observations and their seasonal cycles and the GEOS CCM simulation with emissions-based forcing. *J. Geophys. Res.* **113**, D14302 (2008).
31. Rigby, M. et al. Re-evaluation of the lifetimes of the major CFCs and $CH_3CCl_3$ using atmospheric trends. *Atmos. Chem. Phys.* **13**, 2691–2702 (2013).
32. Hamilton, K. & Fan, S.-M. Effects of the stratospheric quasi-biennial oscillation on long-lived greenhouse gases in the troposphere. *J. Geophys. Res.* **105**, 20581–20587 (2000).
33. Simmonds, P. G. et al. Interannual fluctuations in the seasonal cycle of nitrous oxide and chlorofluorocarbons due to the Brewer-Dobson circulation. *J. Geophys. Res.* **118**, 10694–10706 (2013).
34. Nevison, C. D. et al. Exploring causes of interannual variability in the seasonal cycles of tropospheric nitrous oxide. *Atmos. Chem. Phys.* **11**, 3713–3730 (2011).

a

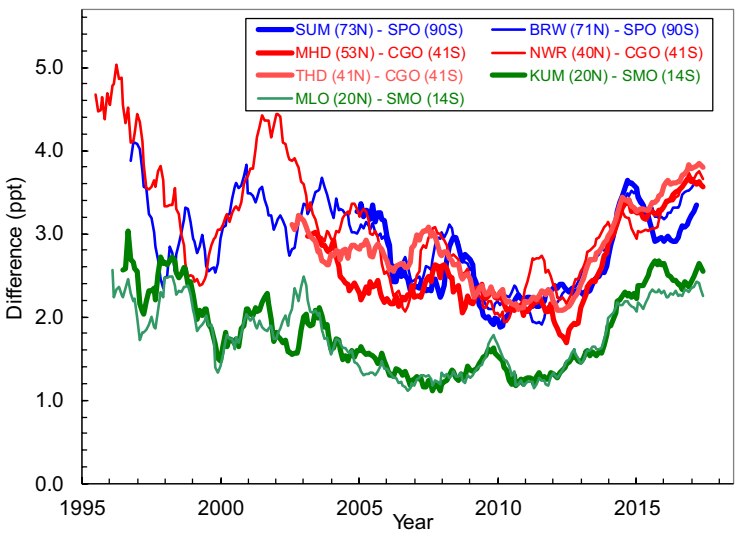


b

| *Site* | *Code* | *Latitude* | *Longitude* | *Altitude* (m)* | *Methods*** |
|---|---|---|---|---|---|
| South Pole, Antarctica | SPO | 90°S | | 2837 | I, F |
| Palmer Station, Antarctica | PSA | 64.6°S | 64.0°W | 15 | F |
| Cape Grim, Australia | CGO | 40.682°S | 144.688°E | 164 | F |
| American Samoa | SMO | 14.247°S | 170.564°W | 77 | I,F |
| Mauna Loa, USA | MLO | 19.5362°N | 155.5763°W | 3433 | I,F |
| Cape Kumukahi, USA | KUM | 19.516°N | 154.811°W | 39 | F |
| Niwot Ridge, USA | NWR | 40.0518°N | 105.5854°W | 3523 | I,F |
| Trinidad Head, USA | THD | 41.054°N | 124.151°W | 120 | F |
| Mace Head, Ireland | MHD | 53.3°N | 9.9°W | 42 | F |
| Barrow, USA | BRW | 71.323°N | 156.611°W | 27 | I,F |
| Alert, Canada | ALT | 82.5°N | 62.3°W | 210 | F |
| Summit, Greenland | SUM | 72.6°N | 38.4°W | 3209 | I,F |

* altitudes represent the sample inlet location, in meters above sea level.
** I = GCECD in-situ instrument making ongoing measurements multiple times per day.
F = from flasks collected approximately weekly that are measured at the NOAA labs in Boulder by GCECD and GCMS.

**Extended Data Fig. 1 | Hemispheric differences in CFC-11 mole fractions represented by results from individual sites at comparable latitudes. a**, Twelve-month running means of monthly differences are plotted at the mid-point of that time interval. Results from low latitudes (green lines) include a site at high-altitude (MLO) and low-altitude (KUM) in the Northern Hemisphere compared to the site at American Samoa (SMO). Results from mid- to high-latitude site pairs are indicated in other colours and include data from high-altitude (NWR, SUM, SPO) and low-altitude (THD, MHD, BRW) sites. Comparisons made at sites with similar sampling altitudes are indicated in bold lines. **b**, Details of site locations from which measurements of CFC-11 are obtained from flasks and from in situ instrumentation.

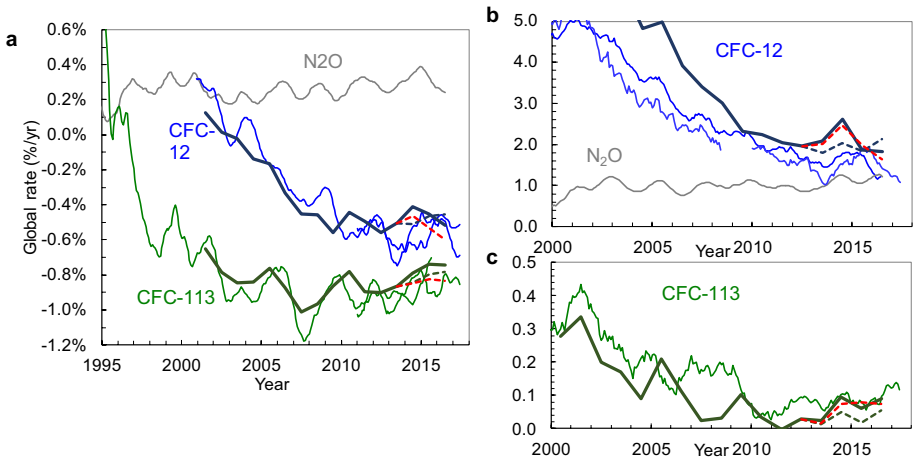


**Extended Data Fig. 2 | Observed and simulated global rates of change and hemispheric differences for some other long-lived chemicals.** **a**, Measured global surface rates for $N_2O$ (grey line), CFC-12 (thin blue lines), and CFC-113 (thin green lines) from flasks analysed by GC–ECD and also, for the CFCs, by GC–MS. **b**, Hemispheric differences measured for CFC-12 and $N_2O$. **c**, Hemispheric differences measured for CFC-113. Multiple CCM simulation results appear in **a**, **b**, and **c** for CFCs as thick dark lines and are updated only annually; they represent simulations using the CAMCHEM model with MERRA2 reanalysis meteorology and the three-box-derived emission history. Dashed lines after 2012 represent simulations with emissions kept constant after 2012 (dark blue for CFC-12 or dark green for CFC-113), or when the three-box-derived emission record was considered but dynamics in 2012 were repeated in subsequent years (red dashed lines). Emission distribution 1 was used in all simulations (see Methods). Interannual variability in global growth rates for these gases are sometimes correlated, suggesting a common cause related to STE dynamics, perhaps associated with the quasi-biannual oscillation, although emission variations are particularly likely for $N_2O$ (for example, refs 32–34). This may explain the peak in growth rates for a number of gases in 2015. The change in rate for CFC-11 (see Fig. 4), however, is substantially larger and is sustained in 2016 when rates for other gases do not change appreciably or become smaller, suggesting that the underlying causes for the majority of changes observed for CFC-11 are unique to that gas.

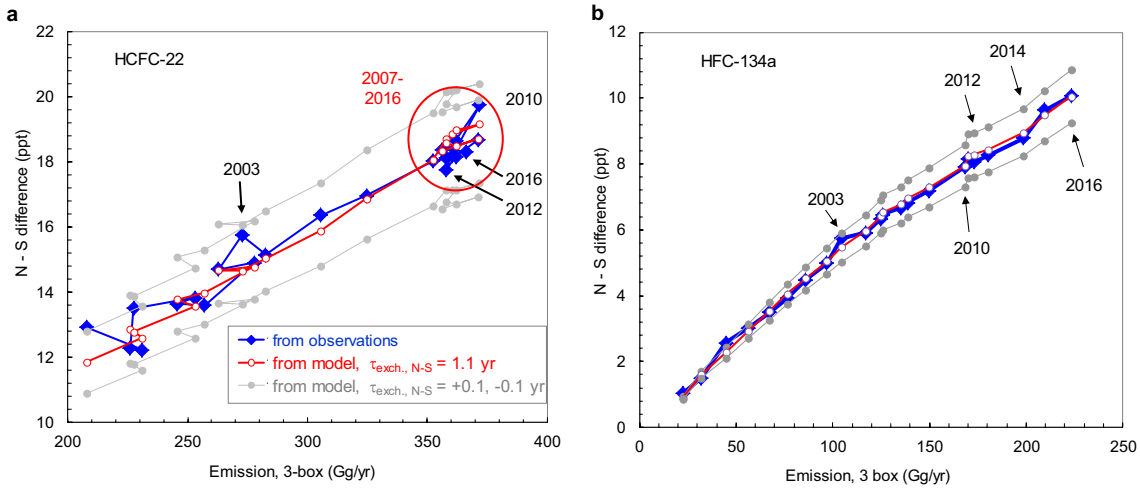


**Extended Data Fig. 3 | The sensitivity of hemispheric mole fraction differences to variations in hemispheric air mass exchange. a**, **b**, Points represent the observation-based (blue symbols) or modelled (red and grey symbols) hemispheric difference as a function of the global emission rate derived for that year in the three-box model for HCFC-22 (**a**) and for HFC-134a (**b**; see Methods; lines connect sequential years and the legend applies to **a** and **b**). The sensitivity of the hemispheric mole fraction difference (N−S difference) to exchange timescale ($\tau_{exch,\,N-S}$) was tested in the model by incorporating values of ± 0.1 yr around 1.1 yr. If this timescale did not vary interannually, we would expect the observation-based points (blue) to overlay those from the model (red). A change in the annual mean value of this exchange would increase the difference between the observed and modelled N−S difference. Specifically, an annual mean change of ± 0.1 year would be reflected in the observed N−S difference being two-thirds of the way closer to the grey point associated with the emission derived for that year. The consistency between the model (red) and observed (blue) hemispheric differences in most years suggests that interannual changes in the exchange timescale are 0.1 yr (around 10%) or less, typically. More importantly, the results show no systematic change in this relationship before and after 2012, suggesting that any change in the rate of hemispheric air exchange in the troposphere is less than 10% during this period. We estimate that to fit the observed increase in the N–S difference measured for CFC-11 after 2012 without increasing the net CFC-11 flux to the Northern Hemisphere, this exchange time constant would have had to increase from 1.1 to 1.7 yr, which is inconsistent with the results presented here. Although the distribution of emissions between and within the hemispheres can affect the N–S difference, any considerable change in this distribution over time would probably be a shift to lower latitudes (away from the US and Europe) and would lead to a decrease in the N−S difference over time, not an increase as is observed for CFC-11 after 2012. Consistent with this, the best fit to the observations was obtained when the emission distribution (North Hemisphere/global) in these analyses was linearly decreased over time (from 0.95 in 1995 to 0.85 in 2015 for HFC-134a, and from 0.86 to 0.82 for HCFC-22). Assuming a constant hemispheric emission distribution (Northern Hemisphere/global) over time does not change the conclusions from this analysis.

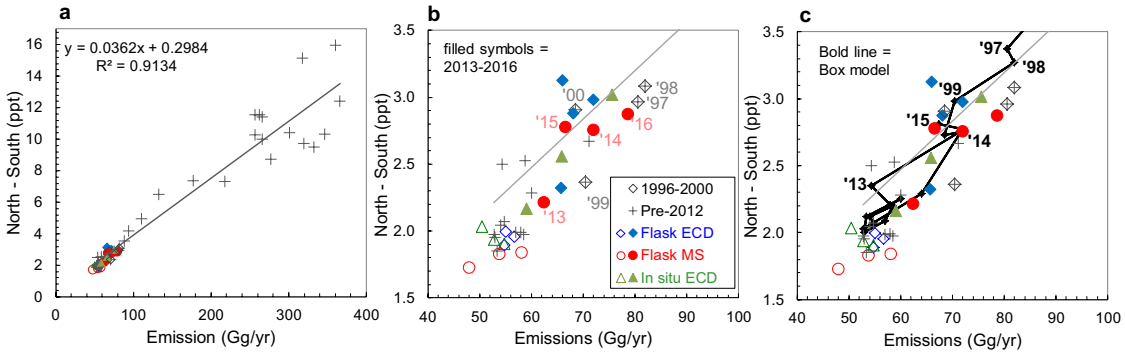


**Extended Data Fig. 4 | Measured and modelled annual hemispheric differences versus global emissions of CFC-11. a**, Measured mole fraction differences between the Northern and Southern Hemispheres (North − South) as a function of the global emission derived with a three-box model for 1978–2016; the line is a fit to all results and each point represents an annual mean difference and emission for a particular year. **b**, An expanded scale of data displayed in **a** with results from different measurement methods represented by symbols of the same colour; grey symbols (plus signs and diamonds) refer to a combined set of results from flasks and in situ instruments analysed by GC–ECD. For each method (colour), unfilled symbols refer to results for the years 2010–2012; filled symbols refer to 2013–2016. Specific years are labelled for GC–MS results during 2013–2016 and for ECD results during 1997–2000 (for example, ’15 is 2015). The data show that the relationship observed here during 2014–2016 is similar to that observed during 1996–2000. **c**, Same as **b**, but with differences between the Northern and Southern Hemispheres derived from the three-box model shown (black points and line connecting sequential years); select model years are labelled.

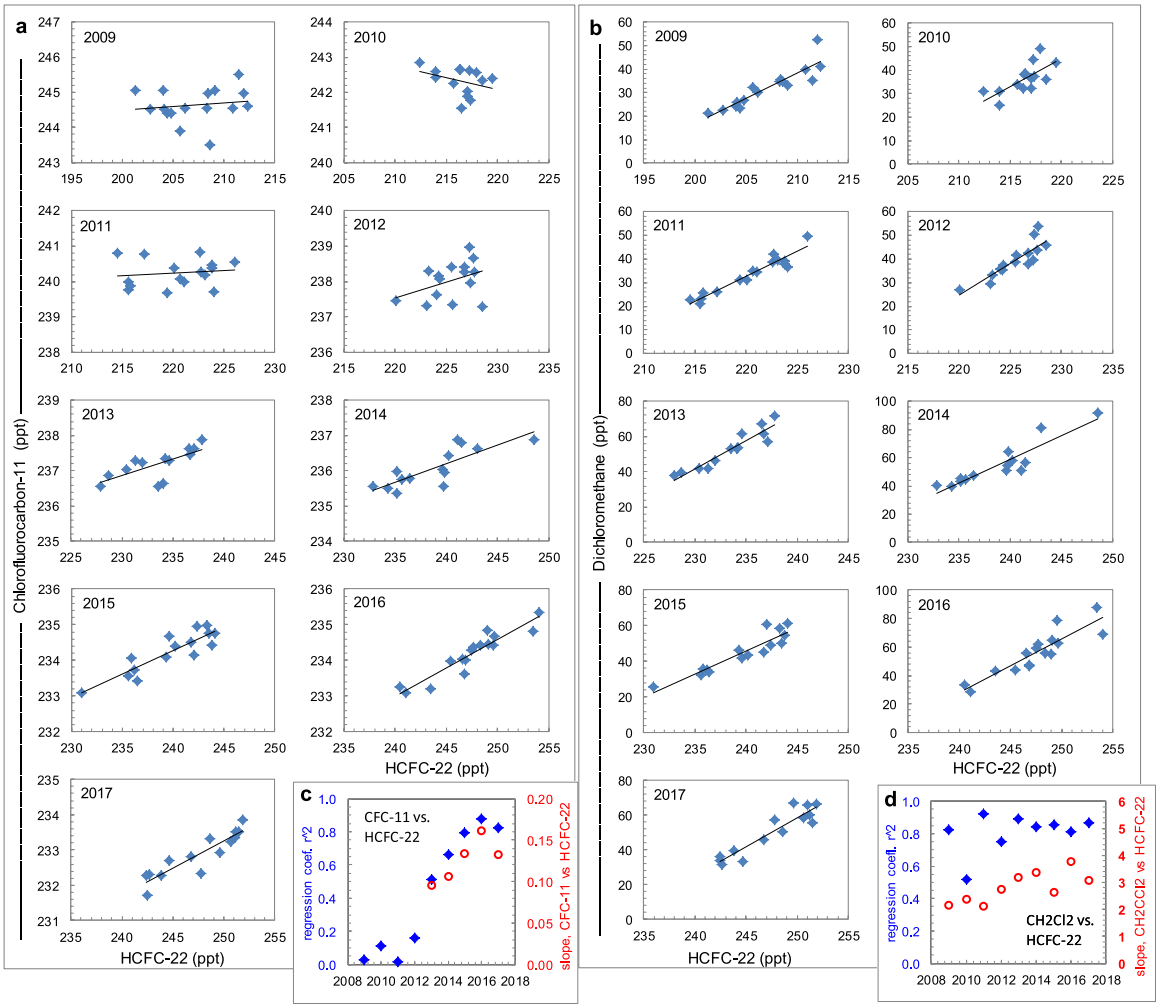


**Extended Data Fig. 5 | Correlations between trace gases measured during autumn at Mauna Loa. a**, Measured mole fractions of CFC-11 and HCFC-22 in all samples collected during autumn (fraction of year $> 0.6$ and $< 0.9$) at MLO in the past nine years. **b**, Results for $CH_2Cl_2$ versus HCFC-22 in those same samples and years. **c**, The $r^2$ regression coefficients (blue filled symbols, left-hand scale) and slopes (red unfilled symbols, right-hand scale) determined from the data in **a** over time. Only slopes for correlations that are significant at $P < 0.05$ are shown (that is, those for which $r^2 > \sim 0.25$). **d**, The same as **c**, but for the data in **b** ($CH_2Cl_2$ versus HCFC-22). Eastern Asia has been a substantial source of HCFC-22 and $CH_2Cl_2$ for a number of years[1,11]. As a result, significant correlated variability is expected in their mixing ratios downwind of this region; this is borne out in observations at MLO during autumn from 2009 to 2017. These data may also provide rough estimates of relative emission magnitudes. For example, inventory- and atmosphere-based studies suggest emissions of HCFC-22 from China of around 100 Gg in 2010, increasing to 150 Gg in 2015 (ref. 1). Considering the slopes measured at MLO between HCFC-22 and $CH_2Cl_2$, this would correspond to regional emissions of $CH_2Cl_2$ of 300 Gg in 2010 increasing to 440 Gg in 2016. This is comparable to the 455 Gg ($\pm$10%) estimated to have been used in China for emissive applications in 2015 (ref. 11). Applying the same analysis to CFC-11 suggests total emissions of 30–40 Gg $yr^{-1}$ for 2014–2017, or 10–35 Gg higher than estimated for Chinese CFC-11 emissions in 2008–2009 (considering errors[1]), which is of the same order as the global CFC-11 emission increase derived here for 2014–2016 ($13 \pm 5$ Gg $yr^{-1}$). Although our data and analyses do not allow for a robust identification of the origin of the increase in CFC-11 emissions, we explore China's potential contribution because it is also the largest producer and user of HCFCs in eastern Asia (see ref. 4 and http://ozone.unep.org/en/data-reporting/data-centre).

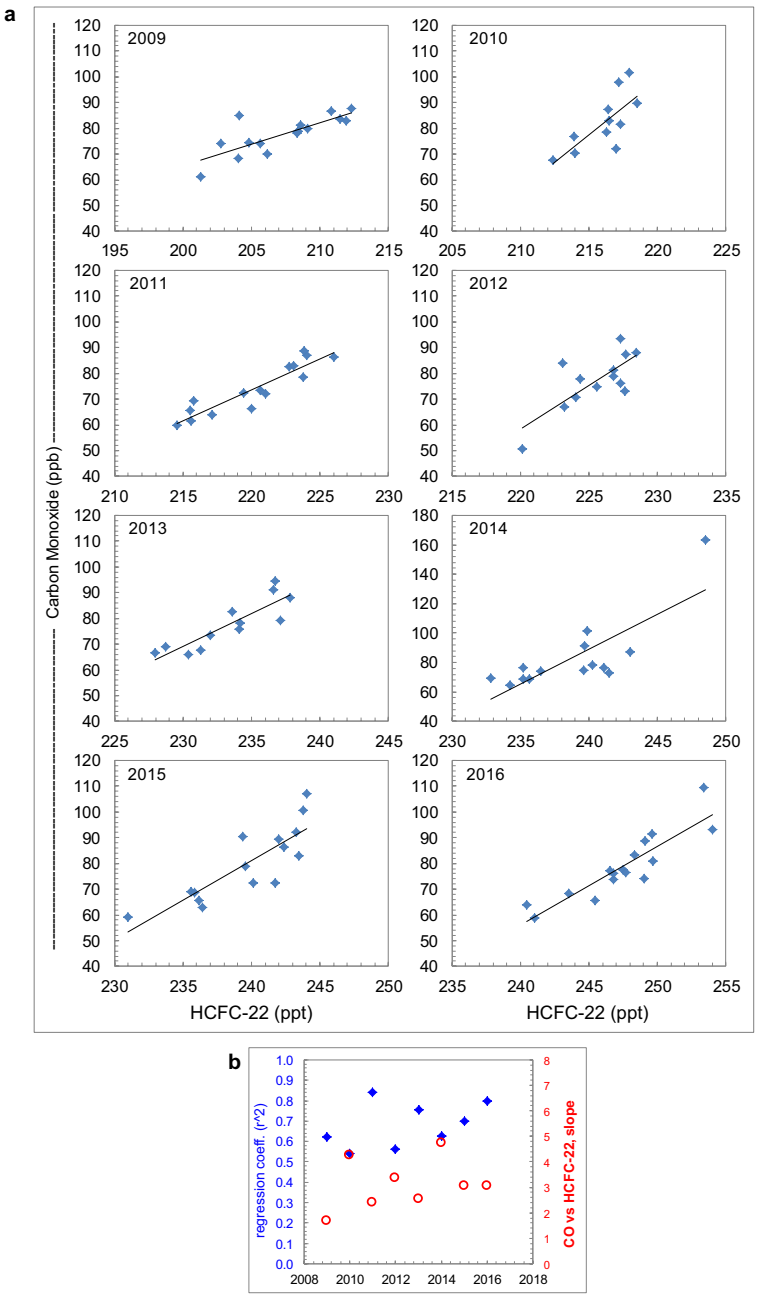


**Extended Data Fig. 6 | Correlations between additional trace gases measured during autumn at Mauna Loa.** Same as Extended Data Fig. 5, but for mole fractions of carbon monoxide versus HCFC-22 measured at MLO during autumn. **a**, The results in individual years. **b**, The $r^2$ regression coefficients (blue filled symbols, left-hand axis) and slopes (red unfilled symbols, right-hand axis) determined from the data in **a** over the past eight years.

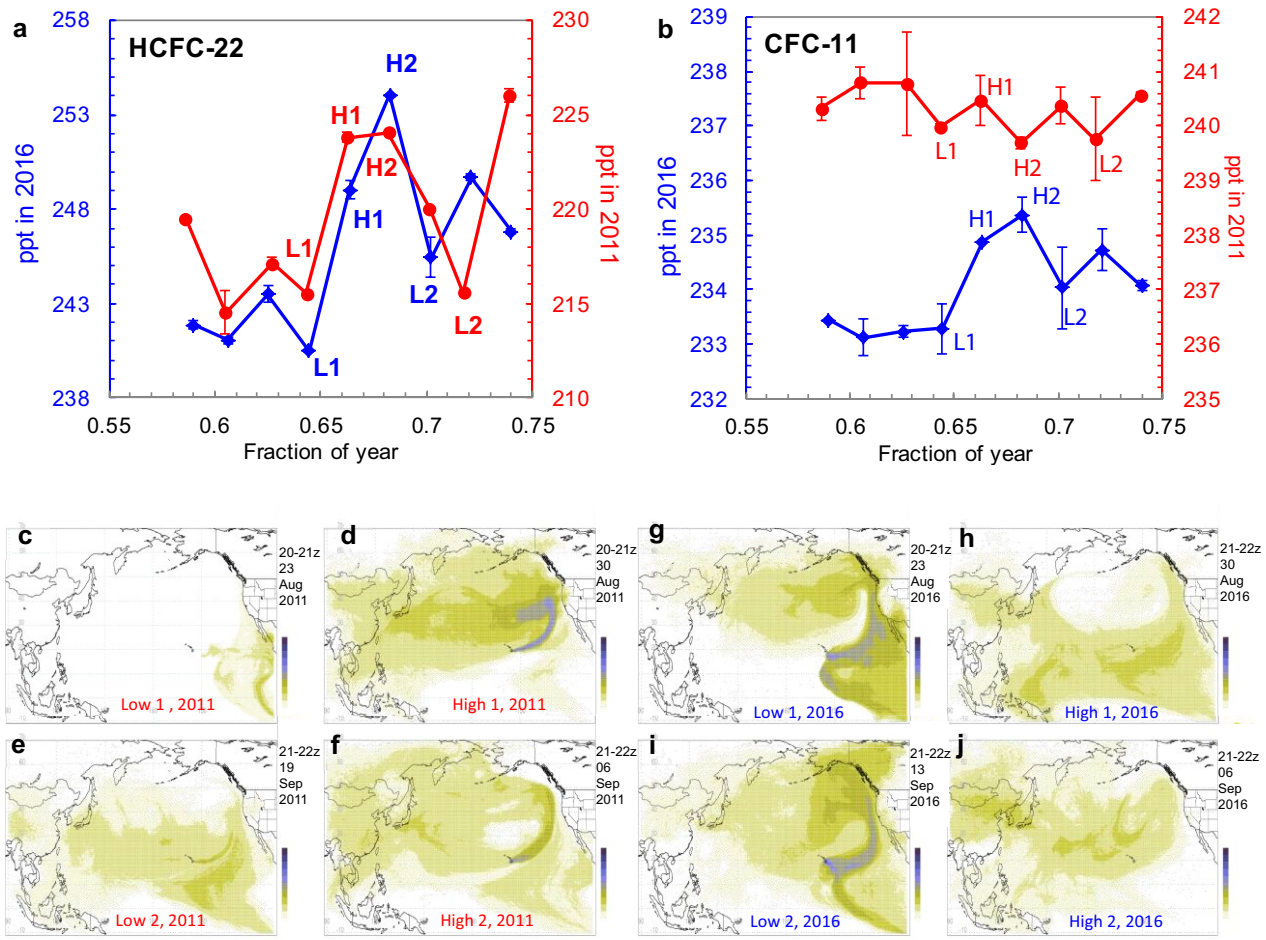


**Extended Data Fig. 7 | Variability in trace gas mole fractions measured at MLO before and after 2012. a**, Mole fractions of HCFC-22 measured in flasks collected at MLO during the autumn of 2011 (red lines and symbols) and 2016 (blue lines and symbols). **b**, The same as **a**, but for CFC-11. **c**–**f**, Back trajectories calculated[27] for 2011 samples indicated by the red text L1, L2, H1 and H2 in **a** and **b**. **g**–**j**, Back trajectories calculated for 2016 samples indicated by the blue text L1, L2, H1 and H2 in **a** and **b**. In **c**–**j**, darker shading represents surface regions sensed by the corresponding sampling events at MLO, with darker colours indicating greater influence. The colour scale in the trajectory maps is logarithmic ($1 \times 10^{-9}$ to $1 \times 10^{-3}$ g s m$^{-3}$, darker colours for higher concentrations) and represents the calculated time-averaged concentration within the 0–2,000 m surface layer during the 30 days before the sampling event given a point release at MLO[27] of 1 g s$^{-1}$. Increased mole fractions of HCFC-22 are observed in both 2011 and 2016 (labelled H1 and H2 in **a** or **b** and High 1 and High 2 in **c**–**j**) when surface sensitivity over eastern Asia is enhanced; CFC-11 mole fractions at MLO co-vary with HCFC-22 in these eastern-Asian influenced samples only after 2012. Some industrialized regions (for example, Japan) have considerable influence on samples containing both high and low mole fractions of CFC-11, HCFC-22 and $CH_2Cl_2$ and, therefore, are less likely to be the source of the greater mole fractions of CFC-11 at MLO after 2012. These results, along with results from Fig. 3 and Extended Data Figs. 5 and 6, suggest an increase in CFC-11 emissions from eastern Asia that is coincident with the increase in global emissions derived from our sampling network.

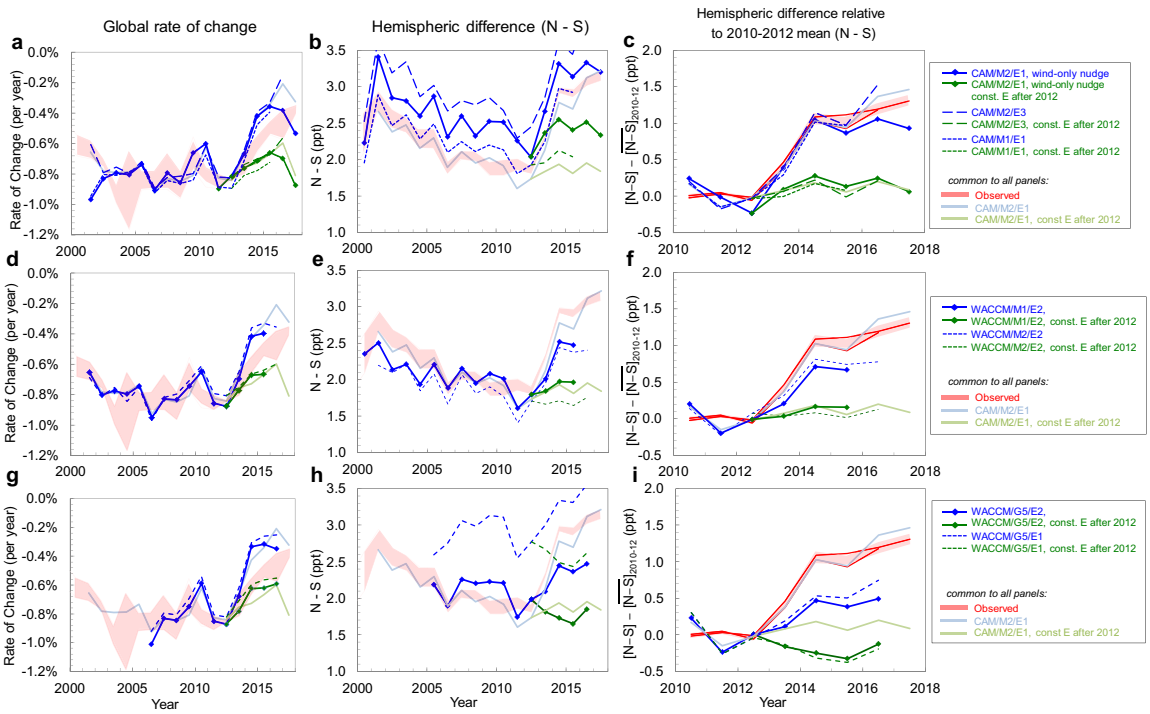


**Extended Data Fig. 8 | Additional model simulations of the changes in CFC-11 mole fraction over time and of hemispheric differences.** Rates of change and hemispheric differences from different combinations of emission distributions (E1, E2, E3), reanalysis meteorology (MERRA1 (M1), MERRA2 (M2), and GEOS5 (G5)), and CCMs (CAM and WACCM) are compared to quantities derived from observations (red lines or shading indicate the range of results from two (hemispheric differences) or three (global change rates) measurement techniques (Methods)). In all panels, results from observations and the CAM run using the Emission1 distribution and MERRA2 reanalysis meteorology are shown for reference (solid light blue and green lines). All blue lines represent simulations using the emission record derived from the three-box model analysis of observations, whereas all green lines indicate simulations with emissions kept constant after 2012 at the 2012 rate. **a**–**c**, Results from CAM as a function of emission distribution (E1 and E3) and nudging methodology (temperature and winds, or wind-only). **d**–**f**, Results from WACCM as a function of reanalysis meteorology (MERRA1 or MERRA2). **g**–**i**, Results from WACCM with GEOS5 reanalysis meteorology and two different emission distributions (E2 and E1). The comparisons are made for the CFC-11 global rate of change at the Earth's surface (**a**, **d**, **g**; left column), the surface mean hemispheric difference (**b**, **e**, **h**; middle column), and the change in the surface mean hemispheric difference relative to the mean during 2010–2012 (**c**, **f**, **i**; right column; note expanded time axis). All quantities being compared are derived from hemispheric means determined from cosine of latitude weighting of observed or simulated mole fractions at sampling locations (Methods).

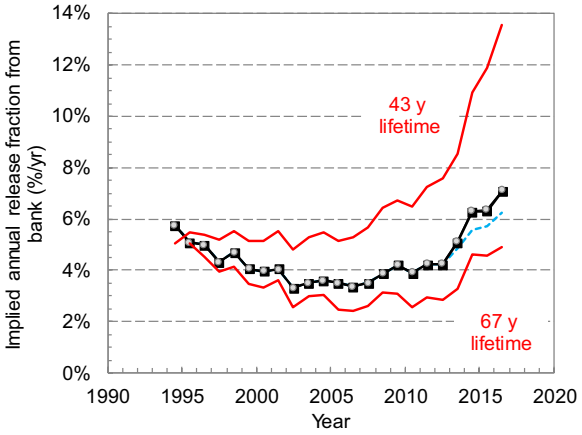


**Extended Data Fig. 9 | The sensitivity of derived bank release rates to CFC-11 lifetime and incineration.** Bank release rates derived with a 57.5-year lifetime as shown in Fig. 2b (black squares and the dashed blue line) are also calculated considering the upper and lower values for the most likely CFC-11 lifetime range (red lines; 43–67 yr, ref. 1). Including quantities of CFC-11 destroyed (for example, by incineration) reported to UNEP (grey circles) affect this result minimally.

**Extended Data Table 1 | Derived global emissions and global production of CFC-11**

| *Year* | *Emis. 3-box* | *1 s.d.* | *Emis. 12-box* | *Low* | *High* | *Production*[a] |
|---|---|---|---|---|---|---|
| 1994 | 103.9 | 4.6 | 81.2 | 7.5 | 6.1 | 99.8 |
| 1995 | 92.0 | 4.5 | 79.5 | 6.3 | 7.0 | 72.6 |
| 1996 | 89.0 | 4.3 | 94.3 | 5.6 | 6.3 | 55.9 |
| 1997 | 75.8 | 3.5 | 79.4 | 6.6 | 6.1 | 62.5 |
| 1998 | 81.7 | 3.0 | 78.5 | 5.6 | 6.6 | 54.3 |
| 1999 | 69.5 | 2.6 | 68.1 | 4.4 | 3.9 | 54.1 |
| 2000 | 67.3 | 3.1 | 65.5 | 3.3 | 3.7 | 44.1 |
| 2001 | 67.7 | 5.6 | 66.7 | 3.0 | 2.6 | 32.2 |
| 2002 | 54.4 | 2.1 | 48.9 | 2.7 | 3.0 | 31.8 |
| 2003 | 56.5 | 6.5 | 56.4 | 3.4 | 2.9 | 25.5 |
| 2004 | 56.9 | 5.1 | 55.2 | 3.6 | 3.7 | 22.3 |
| 2005 | 54.4 | 5.1 | 57.6 | 3.3 | 3.5 | 13.9 |
| 2006 | 50.8 | 2.4 | 49.9 | 3.3 | 3.2 | 10.9 |
| 2007 | 51.6 | 2.0 | 56.6 | 2.9 | 3.6 | 2.8 |
| 2008 | 54.9 | 5.0 | 54.9 | 3.9 | 3.2 | 1.4 |
| 2009 | 57.4 | 2.2 | 53.7 | 3.6 | 4.1 | 0.9 |
| 2010 | 51.1 | 4.7 | 50.9 | 3.4 | 3.7 | 0.4 |
| 2011 | 53.2 | 3.5 | 53.9 | 3.4 | 3.9 | 0.1 |
| 2012 | 50.9 | 2.3 | 53.4 | 3.6 | 3.7 | 0.3 |
| 2013 | 58.7 | 5.3 | 54.3 | 3.8 | 3.7 | 0.0 |
| 2014 | 68.9 | 2.3 | 68.8 | 3.9 | 4.1 | 0.1 |
| 2015 | 64.8 | 2.2 | 64.9 | 3.8 | 3.9 | -- |
| 2016 | 68.0 | 6.4 | 67.2 | 4.5 | 4.1 | -- |

All values in Gg $y^{-1}$.

[a]Total CFC-11 production reported to the UNEP Ozone Secretariat. The Montreal Protocol requires that all CFC production be reported to the Ozone Secretariat, including production for dispersive and non-dispersive uses, production for use as chemical intermediates or feedstocks, and any unintentional by-production. No subtractions for reported destruction amounts are included in these values; cumulative destruction of CFC-11 reported to the Ozone Secretariat totalled 16 Gg in all years since 1998 (ref. 4).